Differentiation signals from glia are fine-tuned to set neuronal numbers during development

Anadika R. Prasad[1]†, Matthew P. Bostock[1]†, Inês Lago-Baldaia[1], Zaynab Housseini[1] and Vilaiwan M. Fernandes[1]*.

[1]Department of Cell and Developmental Biology, University College London, Gower Street, London, WC1E 6DE.

†These authors contributed equally to the work.

*Corresponding author; vilaiwan.fernandes@ucl.ac.uk

Abstract

Precise neuronal numbers are required for circuit formation and function. Known strategies to control neuronal numbers involve regulating either cell proliferation or survival. In the developing *Drosophila* visual system photoreceptors from the eye-disc induce their target field, the lamina, one column at a time. Although each column initially contains ~6 precursors, only 5 differentiate into neurons of unique identities (L1-L5); the 'extra' precursor undergoes apoptosis. We uncovered that Hedgehog signalling patterns columns, such that the 2 precursors experiencing the lowest signalling activity are specified as L5s; only one differentiates while the other 'extra' precursor dies. We showed that a glial population called the outer chiasm giant glia (xg^O), which reside below the lamina, relays differentiation signals from photoreceptors to induce L5 differentiation. The precursors nearest to xg^O differentiate into L5s and antagonise inductive signalling to prevent the 'extra' precursors from differentiating, resulting in their death. Thus, tissue architecture and feedback from young neurons fine-tune differentiation signals from glia to limit the number of neurons induced.

Introduction

Many sensory systems consist of repeated circuit units that map stimuli from the outside world onto sequential processing layers[1]. It is critical that both absolute and relative neuronal numbers are carefully controlled for these circuits to assemble with topographic correspondence across processing layers. Neuronal numbers can be set by controlling how many progeny a neural stem cell produces, or by regulating how many neural progeny survive[2,3]. To investigate other developmental strategies that set neuronal numbers, we used the highly ordered and repetitive *Drosophila melanogaster* visual system. Like vertebrate visual systems, the fly visual system is organized retinotopically into repeated modular circuits that process sensory input from unique points in space spanning the entire visual field[4,5].

Retinotopy between the compound eye and the lamina is built during development. Photoreceptors are born progressively in the eye imaginal disc as a wave of differentiation sweeps across the tissue from posterior to anterior. Newly born photoreceptors express Hedgehog (Hh), which promotes further wave propagation[6]. They also express the Epidermal Growth Factor (EGF), Spitz (Spi), which recruits additional photoreceptors into developing ommatidia[6]. As photoreceptors are born, their axons project into the optic lobe and induce the lamina, such that there is a corresponding lamina unit (called a cartridge) for every ommatidium (Fig. 1A)[4]. Each cartridge is composed of five interneurons (L1-L5; named for the medulla layers they project to) and multiple glial subtypes[4,7].

Lamina induction is a multi-step process triggered by photoreceptor-derived signals. Photoreceptor-derived Hh converts neuroepithelial cells into lamina precursor cells (LPCs), promotes their terminal divisions and orchestrates lamina column assembly, *i.e.* the stacked association of ~6 post-mitotic LPCs with photoreceptor axon bundles (Fig. 1A,B)[8–11]. Once assembled into columns, LPCs differentiate into neurons following an invariant spatio-temporal pattern whereby the most proximal (bottom) and most distal (top) cells differentiate first into L5 and L2, respectively; differentiation then proceeds in a distal-to-proximal (top-to-bottom) sequence, L3 forming next, followed by L1, then L4[12–14]. The sixth LPC, located between L4 and L5, does not differentiate but instead is fated to die by apoptosis and is later cleared (Fig. 1A)[15]. Previously we showed that a population of glia called wrapping glia, which ensheath photoreceptor axons, induce neuronal differentiation of L1-L4 neurons via Insulin/ Insulin-like growth factor signalling in response to EGF from photoreceptors[14]. Moreover, L1-L4 neuronal

differentiation could be disrupted by manipulating wrapping glia without affecting L5 differentiation[14]. Indeed, the mechanisms that drive L5 differentiation are not known. Importantly, we do not understand how exactly 5 neuron types differentiate from 6 apparently equal LPCs; in other words, how are lamina neuronal numbers set?

Results

The 'extra' lamina precursor cells are specified as L5s

To probe how only five lamina neurons are invariantly produced from a pool of six seemingly equivalent precursors, we began by focusing on the 'extra' LPCs, which are located distal to L5s[9]. To confirm that these cells do indeed undergo apoptosis in normal development, we used an antibody against the cleaved form of Death Caspase-1 (Dcp-1), an effector caspase, to detect apoptotic cells[16]. In wild-type animals, we detected Dcp-1 positive apoptotic cells in the lamina immediately distal to L5 neurons starting from column 5.15 ±0.25 Standard Error of the Mean (SEM; N=13; Fig. 1C). Note that for these and later analyses we considered the youngest column located adjacent to the lamina furrow to be the first column, with column number (age) increasing towards the posterior (right) side of the furrow (Fig. 1A). Next, we examined the fate of these cells when apoptosis was blocked in animals mutant for *Death regulator Nedd2-like caspase (Dronc)*, an initiator caspase essential for caspase-dependent cell death[17]. Cleaved Dcp-1 was absent in homozygous $Dronc^{I24}$ animals confirming that apoptosis was blocked (N=26; Fig. 1E). Indeed, we detected cells that were positive for the lamina marker Dachshund (Dac) but negative for the pan-neuronal marker Elav between L1-L4 and L5 neurons past column 5, which were never observed in controls (Fig. 1E compared to 1C; N=13). These cells did not express lamina neuron subtype markers Sloppy paired 2 (Slp2) or Brain-specific homeobox (Bsh), which L5s co-express and which individually label L1-L3s and L4s, respectively (Fig. 1D,F)[13,14,18]. Thus, although the 'extra' cells were retained when apoptosis was blocked, they did not differentiate into neurons.

Since retaining the 'extra' LPCs by blocking apoptosis did not reveal their neuronal potential, we sought to force their differentiation. Previously, we showed that MAPK signalling is necessary and sufficient to drive L1-L4 neuronal differentiation[14]. High levels of double-phosphorylated MAPK (dpMAPK), indicative of pathway activity, preceded neuronal differentiation (assessed by Elav expression), not just for L1-L4s, but also for L5s (Fig. 1G;

N=7), suggesting that MAPK signalling is involved in differentiation for all neuronal types. Therefore, we hyperactivated the pathway by using a lamina-specific Gal4 to drive an activated form of MAPK ($MAPK^{ACT}$) or of a transcriptional effector of the pathway, Pointed P1 (PntP1). Importantly, we combined this Gal4 with a temperature sensitive form of Gal80, $Gal80^{ts}$, to restrict expression during development; this driver is referred to as *Lamina*^{ts} henceforth (Fig. S1C,D and Fig. 1H,I). As reported previously, hyperactivating MAPK signalling in the lamina led to premature neuronal differentiation: instead of sequential differentiation of L1-L4, seen as a triangular front, most lamina columns differentiated simultaneously (Fig. 1H, N=17, Fig. S1A,C, N=10)[14]. We observed no LPCs that remained undifferentiated (Dac^+ and $Elav^-$) past lamina column 5, including the row of cells just distal to L5s (Fig. 1H, S1A,C). Interestingly, we also observed a concomitant decrease in cleaved Dcp-1 positive cells (Fig. 1H, J), suggesting that forcing the 'extra' LPCs to differentiate blocked their death.

We next asked which lamina neuron subtype the 'extra' LPCs could give rise to when induced to differentiate. Using Slp2 and Bsh to distinguish between lamina neurons, we often observed two rows of cells co-expressing Slp2 and Bsh in the proximal lamina (Fig. 1I, S1B,D), indicating the presence of ectopic L5s. However, the presence of ectopic cells could be due to premature differentiation, rather than ectopic induction of a particular cell type. In control animals, columns are fully differentiated (Elav+) from column 7 onwards (Fig. S1E). Therefore, to distinguish between premature and ectopic differentiation, we quantified the number of lamina neuron types (L1-L3, L4 and L5) per column from column 7 onwards. While there was no significant difference between the average number of L1-L3s or L4s per column, the average number of L5s/column was ~1.4-fold higher in laminas in which differentiation was ectopically induced compared with controls (Figs. 1K,L). Thus, hyperactivating MAPK signalling in the lamina drives ectopic differentiation of L5 neurons. Importantly, ectopic L5s were only observed in the proximal but never in the distal lamina (Fig. 1I, N=18/18; Fig. S1D, N=9/9). Taken together, the absence of cell death in the row proximal to L5s and the presence of ectopic L5s in this row indicate that hyperactivating MAPK signalling induces the 'extra' LPCs to differentiate into L5s. Thus, LPCs are not equivalent as previously assumed; instead, they are patterned with fixed neuronal identities along the distal to proximal axis, such that the two most proximal rows of LPCs are specified as L5s and differentiate accordingly when induced.

Hh signalling patterns lamina precursor cells

To uncover how regional differences in LPC specification arise, we integrated published single-cell RNA sequencing datasets for developmental timepoints that span lamina development[19–21] (Fig. S2A; See Materials and Methods). As published previously, on uniform manifold approximation and projection (UMAP) visualizations L1, L2, L3 and L4 neuronal clusters were closer to each other than they were to the L5 cluster[20]. The LPC cluster was connected to differentiated neurons by two streams or tails of cells - one leading to the L1-L4 clusters and the other leading to the L5 cluster (Fig. 2A). Such convergent tails in UMAP visualizations are thought to represent intermediate states between progenitors and differentiated cells, suggesting that L1-L4 and L5 neurons have distinct developmental trajectories from a common pool of LPCs[19,20]. We considered the possibility that these data could support a model proposed previously whereby L5 neurons have a distinct developmental origin to the L1-L4 neurons[22] (See supplementary text). To test this possibility, we used mitotic recombination to label the lineages of neuroepithelial cells with low induction frequency. These resulted in compact patches of lamina cells being labelled, indicating that there is relatively little cell mixing (Fig. S2B,C; 13/13 clones). Importantly, the lineages of individual neuroepithelial cells contained all the lamina neuron types, including L5s, thus indicating that all lamina neurons have the same developmental origin (Fig. S2B,C; 13/13 clones; See Supplementary text).

We asked what transcripts distinguished L5 precursors from L1-L4 precursors, and, surprisingly, we found that several well-established Hh signalling targets were expressed at higher levels in the L1-L4 tail compared with the L5 tail, suggesting the L5 precursors experience lower Hh signalling than other lamina precursors. These included the direct transcriptional target *patched (ptc),* as well as *single-minded (sim), rhomboid (rho)* and *Zn finger homeodomain 1 (zfh1)* (Fig. 2B,C,D and E)[11,23–25]. Indeed, a transcriptional reporter for *ptc (ptc-lacZ)* was expressed at lower levels in L5 neurons compared with L1-L4 neurons (Fig. 2F, S2D). Consistent with the transcriptomic data, *ptc* expression eventually decreased in older neurons (Fig. 2B,F, S2D). Importantly, in young columns prior to neuronal differentiation, *ptc-lacZ* expression was highest in the distal lamina and decreased towards the proximal lamina (quantified in Fig. S2D with summary statistics from a mixed effects linear model in Table S1). Sim expression showed a similar distribution (Fig. S2E). These data indicate that Hh signalling levels are highest in the distal lamina and lowest in the proximal lamina.

Hh signalling is known to trigger the early steps of lamina development, including the expression of early lamina markers such as *dac* and *sim*, terminal LPC divisions and column assembly[8–11], but no role for Hh in lamina neuron specification or differentiation has been identified. We wondered whether Hh signalling could specify neuronal identity in LPCs; specifically, we hypothesised that low Hh signalling levels specify LPCs which will give rise to L5s. To test this, we disrupted Hh signalling using a temperature sensitive allele of *hh* (hh^{ts2}). We raised homozygous mutant hh^{ts2} animals at the permissive temperature (18ºC) and then shifted them to the restrictive temperature (29ºC) for either 6, 12, 24, 45 or 72 hours before dissecting at the white prepupa stage (Fig. 2G-M). Consistent with the known role of Hh signalling in early lamina development, we recovered fewer and fewer lamina neurons with increasing lengths of temperature shifts (Fig. S2F), with no LPCs or L-neurons recovered for the 45- and 72-hour temperature shifts ($N^{45h\text{-}ts}$=10; $N^{72h\text{-}ts}$=10; Fig. 2L,M) [8]. However, for the 6-, 12- and 24-hour temperature shifts, we observed cells expressing the markers Slp2 and Bsh either individually or in combination (Figs. 2I-K). In these brains, we observed Slp2 and Bsh co-expressing cells in higher proportions relative to the total number of neurons (Elav+ cells) with increasing temperature shift lengths, until at the 24-hour temperature shift, nearly all the neurons present were L5s (Fig. 2I-K; quantified in Fig. 2N; $N^{6h\text{-}ts}$=14; $N^{12h\text{-}ts}$=12; $N^{24h\text{-}ts}$=17). Importantly, under these conditions L5s were no longer confined to the proximal lamina but were also observed in distal positions (Fig. 2I-K). These experiments indicate that reducing Hh signalling leads to an increased number of L5s in the lamina, at the expense of other lamina neuron types.

Since Hh is also required for photoreceptor development, we sought to disrupt Hh signalling cell autonomously in the lamina and assess the effects on lamina neuron specification. To this end, we expressed a repressor form of the transcriptional effector of Hh signalling, Cubitus interruptus ($Ci^{repressor}$)[26] in the lamina (Fig. 2O). This led to a higher proportion of Bsh- and Slp2-positive L5s being present relative to other lamina neuron subtypes. In these brains, L5s were distributed throughout the distal-proximal axis and no longer restricted to the proximal lamina (Fig. 2O, N=10). Similarly, knocking down Ci in the lamina by RNA interference (Ci^{RNAi}) (Fig. S2G; N=11) or mis-expressing the kinesin-family protein Costal 2 (Cos2) (Fig. S2H; N=14), which increases processing of full-length Ci to its repressive form[27], resulted in ectopic L5s. Thus, decreasing Hh signalling autonomously within LPCs led to the production of L5 neurons distributed throughout the distal-proximal axis at the expense of other lamina neuron types.

Since reducing Hh signalling resulted in ectopic L5s, we next asked whether increasing Hh signalling autonomously in the proximal lamina would disrupt L5 specification and generate ectopic neurons with distal identities (*i.e.* L2/L3). We induced gain-of-function in Hh signalling by generating positively-labelled clones[28] that were homozygous mutant for a null allele of *ptc,* which encodes a negative regulator of the pathway[23,27]. Homozygous *ptc* mutant clones never contained L5s (Slp2 and Bsh co-expressing cells) but instead only contained neurons singly positive for Slp2, indicative of L2/L3 identity (Fig. 2P; 17/17 clones from 15 optic lobes). Thus, increasing Hh signalling in the proximal lamina results in L2/L3 specification at the expense of L5 specification. In summary, we have identified an unexpected role for Hh signalling levels in LPCs, such that L5s can only be specified if Hh activity is low, and only L2/L3s can be specified when Hh activity is high.

Outer chiasm giant glia (xg^O) induce L5 neuronal differentiation in response to EGF from photoreceptors

The two most proximal rows of LPCs experience low levels of Hh signalling and consequently can give rise to L5s when induced to differentiate; in normal development, one row is fated to produce L5s, while the other is fated to die. This led us to ask what induces only the most proximal LPC row to differentiate into L5s, while the adjacent distal row is eliminated. Since we showed previously that wrapping glia induce L1-L4 neuronal differentiation in response to EGF from photoreceptors, but that L5 differentiation proceeded normally in these conditions[14], we speculated that another glial population may be involved in inducing L5 differentiation in response to EGF from photoreceptors. To test this hypothesis, we blocked EGFR signalling in all glia using a pan-glial driver. This led to a complete block in lamina neuron differentiation as seen by the absence of any Elav positive cells, though LPCs (Dac+ cells) still formed and assembled into columns (Fig. 3A,B). Thus, EGFR activity in a glial population other than the wrapping glia is required for L5 neuronal differentiation.

Since many glial types infiltrate the lamina (Fig. S3A)[29,30], we performed a screen using glia subtype-specific Gal4s to block EGFR signalling and evaluated the presence of L5s by Elav expression (Fig. S3B-M; summarised in Table S2). Blocking EGFR signalling in the outer chiasm giant glia (xg^O) led to a dramatic reduction in the number of L5s (Fig. 3C,D, S3N; See Supplementary text). The xg^O are located below the lamina plexus, often with just one or two

cells spanning the entire width of the lamina. While the xg^{O} extend fine processes towards the lamina, they do not appear to contact LPCs or L5 neurons (Fig. S3O). Moreover, blocking EGFR signalling in the xg^{O} did not affect xg^{O} numbers or morphology (Fig. 3C,D, S3O-R). To test whether L5 neurons specifically were lost when EGFR activity was blocked in xg^{O}, we used antibodies against Bsh and Slp2 together with Svp, which marks L1s. We found that the numbers of L5 neurons specifically were decreased, while numbers of all the other neuron types were unaffected (Fig. 3E-G; $P^{L5}<0.0001$, Mann-Whitney U-test). To test whether the absence of L5s did not simply reflect a developmental delay, we examined adult optic lobes using a different L5 neuronal marker, POU domain motif 3 (Pdm3)[13]. Similar to our results in the larval lamina, L5s were mostly absent in the adult lamina when EGFR was blocked in xg^{O} compared with controls (Fig. S3S,T; $N^{exp}=10$; $N^{ctrl}=11$).

The loss of L5 neurons when EGFR was blocked in xg^{O} could be explained either by a defect in neuronal differentiation, or by an earlier defect in LPC formation or recruitment to columns. To distinguish between these possibilities, we counted the number of LPCs per column when EGFR signalling was blocked in xg^{O} compared to controls (Fig. 3H). In columns 1-4, there were no differences in the number of LPCs, indicating that LPC formation and column assembly occurred normally. Thus, although LPCs formed and assembled into columns normally, L5s failed to differentiate; supporting the hypothesis that in response to EGFR activity xg^{O} induce proximal LPC neuronal differentiation into L5s. Importantly, the number of LPCs began to decrease in older columns (column 5 onwards) when EGFR signalling was blocked in xg^{O} (Fig. 3H). This observation suggested that undifferentiated LPCs in the proximal lamina are eliminated by apoptosis, similar to the 'extra' LPCs in controls. Consistently, we observed Dcp-1 positive cells in the most proximal row of the lamina beginning on average in column 5.93 ± 0.18SEM (N=19; Fig. 3I,J). Altogether these results show that EGFR activity in xg^{O} induces the differentiation of L5 neurons, and that proximal LPCs which fail to receive appropriate cues from xg^{O} die by apoptosis.

Since EGFR activity in wrapping glia is triggered by EGF from photoreceptors[14], we tested whether photoreceptor-EGF could also contribute to activating EGFR in xg^{O}. We took advantage of a mutant for *rhomboid 3 (rho3)* in which photoreceptors are specified but cannot secrete Spi from their axons[31], resulting in failure of L1-L4 neurons to differentiate (Fig. 3K; N=9)[14,31]. In addition to disrupted L1-L4 neuronal differentiation, we previously showed that only a few L5

neurons differentiated in *rho3* animals (Fig. 3K; N=9)[14]. To test whether xg^{O} induce L5 neuronal differentiation in response to photoreceptor-EGF, we restored expression of wild-type Rho3 only in photoreceptors in *rho3* mutant animals using a photoreceptor-specific driver (GMR-Gal4). Rho3 function in photoreceptors was sufficient to fully rescue not only L1-L4 neuronal differentiation, as previously reported, but also L5 neuronal differentiation (Fig. 3L; N=8). Thus, similar to wrapping glia for L1-L4s, xg^{O} respond to EGF from photoreceptors to induce proximal LPCs to differentiate into L5 neurons.

Outer chiasm giant glia secrete multiple ligands to induce MAPK-dependent neuronal differentiation of L5s.

We next asked what signals the xg^{O} secrete to induce L5 differentiation. Since autonomously hyperactivating MAPK signalling in LPCs was sufficient to drive ectopic L5 neuronal differentiation (Fig. 1H, I, S1C,D), the signals inducing differentiation likely act upstream of the MAPK signal transduction cascade. We first confirmed that MAPK signalling is both necessary and sufficient to induce neuronal differentiation of L5s, and moreover that reducing MAPK activity results in death of LPCs (See Supplementary text and Figs. S4A-D). Given this requirement, we reasoned that the differentiation signals from xg^{O} must lead to activation of MAPK signalling in proximal LPCs, likely through a Receptor Tyrosine Kinase (RTK). Indeed, blocking EGFR signalling in xg^{O} resulted in decreased dpMAPK levels specifically in the proximal lamina (Fig. S4E compared with 1G). The *Drosophila* genome encodes 22 ligands which activate 10 RTKs upstream of MAPK signalling[32]. To identify the signal(s) secreted by xg^{O}, we overexpressed these ligands and screened for their ability to rescue the loss of L5s caused by blocking EGFR activity in the xg^{O}. To validate this approach, we tested whether autonomously restoring transcriptional activity downstream of MAPK in xg^{O} while blocking EGFR could rescue L5 differentiation. While blocking EGFR in xg^{O} resulted in 7.3% (±1.6SEM) L5s compared to control, co-expressing PntP1 with $EGFR^{DN}$ in xg^{O} rescued L5 numbers to 24.7% (±2.9SEM) of control laminas ($P<0.0001$ compared to EGFR DN alone; Fig. S4F). We then screened 18 ligands based on available reagents (Fig. S4F). Expression of four ligands resulted in statistically significant rescues of L5 numbers (Fig. S4F). To eliminate false positive hits, we examined enhancer trap lines and published reports to determine whether these ligands are expressed in xg^{O} under physiological conditions (See Supplementary text and Fig.

S4G-J). This enabled us to narrow down our hits to two ligands: the EGF Spi and Col4a1, a type IV collagen, which both rescued L5 differentiation resulting in laminas with 17.4% (±1.9SEM) and 19.7% (±2.2SEM) of the control number of L5s, respectively (P^{spi}<0.01 and P^{Col4a1} <0.0005; Figs. 4A-H, S4F). Col4a1 is thought to activate MAPK signalling through its putative receptor, the Discoidin domain receptor (Ddr)[32]. We used an enhancer trap in the *Ddr* locus and observed that *Ddr* was expressed in LPCs (Fig. S4K).

Spi activates EGFR [32], which was shown to be expressed in LPCs[12]. We ruled out the trivial explanation that the rescue of L5 numbers by Spi was caused by autocrine EGFR reactivation in the xg^O, as Spi expression in xg^O did not autonomously rescue dpMAPK nuclear localisation when EGFR signalling was blocked (Fig. S4L). To test whether *spi* expression in xg^O was indeed regulated by EGFR signalling, we measured *spi* mRNA levels using *in situ* hybridisation chain reaction. Disrupting EGFR signalling in xg^O resulted in significantly reduced fluorescence signal for *spi* mRNA in xg^O compared with controls (Figs. S4M-O; P<0.01). Thus, xg^O express *spi* in response to EGFR activity. Moreover, expressing *spi* or *Col4a1* in xg^O in which EGFR signalling was blocked rescued dpMAPK signal in L5s (Fig. S4P,Q), indicating that these ligands, when expressed from xg^O are sufficient to activate MAPK signalling in the rescued L5s.

Next, we tested whether Spi or Col4a1 could induce ectopic L5 differentiation when overexpressed in the xg^O. Expression of either ligand resulted in a 47.6% (±3SEM, P<0.0001) and 12.6% (±4SEM, P<0.01) increase in the number of L5s/column for Spi and Col4a1, respectively (Fig. 4I-K). Thus, Spi and Col4a1 are each sufficient to induce ectopic L5 differentiation when overexpressed in the xg^O. Given these results, we wondered why expressing either factor resulted in an incomplete rescue of L5 differentiation when EGFR was blocked in xg^O. We speculated that expressing Spi or Col4a1 alone may not lead to consistently high levels of MAPK activity to induce neuronal differentiation in the proximal lamina. Therefore, we expressed both ligands together to assay whether they could rescue L5 differentiation when EGFR signalling was blocked in xg^O. Strikingly, this led to an enhanced and statistically significant rescue relative to expressing either one alone, resulting in laminas with 31.2% (±2.9 SEM) of the control number of L5s (P<0.0001; Figs. 4L-P). Altogether, we find that xg^O secrete multiple factors that lead to activation of the MAPK cascade to induce differentiation of L5s in the proximal lamina.

Newly born L5 neurons inhibit differentiation of distal neighbours to set neuronal number

Although the two most proximal rows of LPCs are specified as L5s, signals from the xg^O induce only the most proximal row to differentiate, ensuring that exactly one L5 is present in each lamina column. How this tight control of neuronal number is achieved is perplexing given that xg^O induce differentiation by secreting diffusible factors. One possible mechanism is that newly-induced L5s may limit the ability of more distal LPCs to differentiate, by preventing MAPK activation in neighbouring cells. To test this hypothesis, we examined the expression of *argos* (*aos*), a secreted antagonist of EGFR signalling, and transcriptional target of the pathway[33,34]. An enhancer trap in the *aos* locus, aos^{W11} was expressed in xg^O and differentiating L-neurons, with the highest levels detected in L5s (Fig. 5A). Interestingly, we also noted ectopic L5s in the laminas of aos^{W11} heterozygotes, which could be the result of decreased Aos expression, as aos^{W11} is a loss-of-function allele (Fig. 5A). These observations suggested that Aos could act in L5s as a feedback-induced sink for EGF ligands to limit further differentiation in the columns. To test this hypothesis, we knocked down *aos* by RNAi using a driver expressed in developing L5s specifically[35] (Fig. 5B). We observed a statistically significant ~1.2-fold increase in the number of L5s (Fig. 5C-E; $P<0.0005$). Thus, xg^O induce MAPK activity in the most proximal LPCs, resulting in their differentiation and in the production of the feedback inhibitor Aos. In turn, Aos limits further differentiation in the column by fine-tuning the availability of the differentiation signal Spi, which ensures that only one L5 differentiates per column, and determines the final number of neurons in each lamina column.

Discussion

Appropriate circuit formation and function require that neuronal numbers are tightly regulated. This is particularly important for the visual system, which is composed of repeated modular circuits spanning multiple processing layers. In *Drosophila,* photoreceptors induce their target field, the lamina, one unit at a time, thus, establishing retinotopy between the compound eye and the lamina[8]. Each lamina unit or column in the adult is composed of exactly 5 neurons; however, columns initially contain 6 LPCs. The sixth, or 'extra', LPC, invariantly located immediately distal to the differentiating L5 neuron, is fated to die by apoptosis. Here we show that these LPCs are specified as L5 neurons, effectively doubling the pool of LPCs that can give rise to L5s (Fig. 1). Most developmental strategies described thus far for setting neuronal number

do so by regulating proliferation and/or survival[2]. Here, we have defined a unique strategy whereby L5 neuronal numbers are set by regulating how many precursors from a larger pool are induced to differentiate, followed by programmed cell death of the excess precursors. We showed that a glial population called xg^{O}, which are located proximal to the lamina, secrete multiple ligands (Spi, Col4a1) that activate MAPK signalling in LPCs to induce their differentiation (Fig. 4, S4). The tissue architecture is such that secreted signals from the xg^{O} reach the most proximal row of LPCs first, and therefore these precursors differentiate first. Upon differentiation, these newly induced neurons secrete the Spi antagonist Aos to limit the available pool of Spi and prevent further cells from differentiating (Figs. 5 and 6). Thus, the structure of the tissue together with feedback from newly induced neurons set neuronal number by limiting which and, therefore, how many LPCs are induced to differentiate.

Hh signalling and neuronal identity

While Hh signalling has long been known to instruct the early stages of lamina development, here we uncovered a previously undescribed role for Hh signalling in specifying neuronal identity. Moreover, our results highlight a remarkable similarity with the vertebrate neural tube where graded Sonic Hedgehog (Shh) signalling patterns neural progenitors[36,37]. Exactly how differential Hh signalling levels are achieved along the distal-proximal axis of lamina columns is still mysterious as photoreceptors are the only source of Hh during lamina development[8] and their axons span the length of the lamina. Nonetheless, our observations raise the tantalizing possibility that Hh may act as a morphogen along the distal to proximal axis in the lamina, similar to Shh along the dorsoventral axis of the neural tube[36,37]. An alternative model for how Hh could pattern the lamina is that LPCs may have different levels of Hh signalling levels at birth, leading them to sort into set distal-proximal positions during column assembly through differential adhesion[10,11]. Along with these possibilities, it will also be important to test whether differential Hh signalling levels alone specify all five neuronal identities or whether additional inputs are needed.

Co-ordinating development through glia

We have shown that in addition to the wrapping glia[14], another population of glia, the xg^{O}, also receive and relay signals from photoreceptors to induce neuronal differentiation in the

lamina (Fig. 3K-L). Remarkably, xg^{O} are born from central brain DL1 type II neuroblasts and migrate into the optic lobes to positions below the developing lamina[38,39]. This underscores an extraordinary degree of coordination and interdependence between the compound eye, optic lobe and central brain. Photoreceptor signals drive wrapping glial morphogenesis and infiltration into the lamina[40], thus setting the pace of L1-L4 neuronal differentiation[14]. Defining the signals that enable xg^{O} to navigate the central brain and optic lobe will be a critical contribution to our understanding of how development is coordinated across brain regions.

Tissue architecture sets up stereotyped programmed cell death

In both vertebrate and invertebrate developing nervous systems, programmed cell death is thought to come in two broad flavours: first as an intrinsically programmed fate whereby specific lineages or identifiable progenitors, neurons or glia undergo stereotyped clearance[2,3,41,42], and second as an extrinsically controlled outcome of competition among neurons for limited target-derived trophic factors, which adjust overall cell numbers through stochastic clearance (also known as the neurotrophic theory)[2,3,42,43]. In the lamina, although the LPCs eliminated by programmed cell death are identifiable and the process stereotyped, it does not appear to be linked to an intrinsic programme. Rather, the predictable and stereotyped nature of apoptosis and differentiation are a consequence of stereotyped responses to extrinsic signalling determined by the architecture of the tissue. Thus, our work highlights that stereotyped patterns of apoptosis can arise from extrinsic signalling, suggesting a new mode to reliably pattern development of the nervous system.

In many contexts, neurotrophic factors promote cell survival by activating MAPK signalling[44,45]. In the lamina, MAPK-induced neuronal differentiation and cell survival appear intimately linked. LPCs that do not activate MAPK signalling sufficiently do not differentiate and are eliminated by apoptosis, likely through regulation of the proapoptotic factor Hid, which has been described extensively in flies[46–48]. Thus, here the xg^{O}-secreted ligands Spi and Col4a1, which activate MAPK, appear to be functioning as differentiation signals as well as trophic factors. Col4a1, in particular, may perform dual roles by promoting MAPK activity directly through its receptor Ddr, and perhaps also by limiting Spi diffusivity to aid in localising MAPK activation.

It will be interesting to determine whether the processes described here represent conserved strategies for regulating neuronal number. Certainly, given the diversity of cell types and complexity of tissue architecture in vertebrate nervous systems, exploiting tissue architecture would appear to be an effective and elegant strategy to regulate cell numbers reliably and precisely.

Methods

Drosophila stocks and maintenance:

Drosophila melanogaster strains and crosses were reared on standard cornmeal medium and raised at 25^{O}C or 29^{O}C or shifted from 18^{O}C to 29^{O}C for genotypes with temperature sensitive Gal80, as indicated in Table S3.

We used the following mutant and transgenic flies in combination or recombined in this study (See Table S3 for more details; {} enclose individual genotypes, separated by commas): *{y,w,hsflp^{122}; sp/Cyo; TM2/TM6B}*, *{y,w; sp/Cyo, Bacc-GFP; Dr/TM6C},* (from BDSC: 36349) *{ey-Gal80; sp/Cyo;}* (BDSC: 35822), *{;Gal80^{ts}; TM2/TM6B}* (BDSC: 7108), *{w^{1118};; R27G05-Gal4}* (BDSC: 48073), *{w^{1118};;25A01-Gal4}* (BDSC: 49102), *{y,w; R64B07-Gal4;}* (larval L5-Gal4), {y,w; hh-Gal4/TM3} (BDSC: 67493), *{;tub-Gal80^{ts}; repo-Gal4/TM6B}*, *{w^{1118};GMR-Gal4/Cyo;}* (BDSC: 9146), *{y,w;Pin/Cyo;repo-QF/TM6B}* (BDSC: 66477), *{y,w; NP6293-Gal4/Cyo,UAS-lacZ;}* (perineurial glia; Kyoto Stock Center: 105188), *{w; NP2276-Gal4/Cyo; }* (subperineurial glia; Kyoto Stock Center: 112853), *{w^{1118};; R54H02-Gal4}* (cortex glia; BDSC: 45784), *{w^{1118};; R10C12-Gal4}* (epithelial and marginal glia; BDSC: 47841), *{w;Mz97-Gal4, UAS-Stinger/Cyo;}* (wrapping and xg^{O}; BDSC: 9488), *{w^{1118};; R53H12-Gal4}* (chiasm glia; BDSC: 50456), *{y,w; spi^{NP0289}-Gal4/Cyo, UAS-lacZ;}* (Kyoto Stock Center: 112128), *{w^{1118}; Cg-Gal4;}* (BDSC: 7011), *{w;; bnl^{NP2211}-Gal4}* (Kyoto Stock Center: 112825), *{w; ths^{MI07139}-Gal4/Cyo; MKRS/TM6B}* (BDSC: 77475), *{;;rho3^{PLLb}, UAS-CD8::GFP/TM6B}*, *{;UAS-rho3-3xHA;}* (gifts from B. Shilo), *{;;aos^{w11}/TM6B}* (*aos-lacZ*; BDSC: 2513), *{y,w;;hh^{ts2}/TM6B}*, *{y,w; ptc-lacZ/Cyo;}* (BDSC: 10514), *{y,w; sp/Cyo, Bacc-GFP; 10xQUAS-6xmCherry-HA}* (BDSC: 52270), *{y,w;;10xUAS-myrGFP}* (BDSC: 32197), *{;UAS-CD8::GFP;}*, *{;;UAS-CD8::GFP}* (gifts from C. Desplan), *{y,w;;UAS-nls.lacZ},* (BDSC: 3956), *{y,w; UAS-LifeAct-GFP/Cyo;}* (BDSC: 35544), *{w^{1118};UAS-Dcr-2;}* (BDSC: 24650), *{w^{1118};;UAS-Dcr-2}* (BDSC: 24651), *{;UAS-EGFR^{DN}; UAS-EGFR^{DN}}* (BDSC: 5364), *{;UAS-aop^{ACT};}* (Kyoto Stock Center:

108425), *{y,w;UAS-rl^{sem};}* (rl^{sem} = MAPK^{ACT}; BDSC: 59006), *{w^{1118};;UAS-PntP1}* (BDSC: 869), *{w^{1118};UAS-aos^{RNAi};}* (VDRC47181), *{y,w;;UAS-Ci^{76}/TM6B}* (Ci^{76} = Ci^{repressor}; a gift from J. Treisman), *{y;;UAS-Ci^{RNAi}}* (BDSC: 64928), *{w; UAS-cos; MKRS/TM6B},* (Cos2 or Costa; Cos; BDSC: 55039), *{w;UAS-jeb;}* (a gift from A. Gould), *{y,w, UAS-Col4a1^{EY11094}/(Cyo);}* (BDSC: 20661), *{;;UAS-Cg25c-RFP}* [49] *(Col4a1 = Cg25c)*, *{;UAS-Wnt5;}* (BDSC: 64298), *{;;UAS-s.spi}* (a gift from B. Shilo), *{;UAS-m.spi::GFP-myc;}* (a gift from B. Shilo), *{;;UAS-m.spi::GFP-myc}* (a gift from B. Shilo), *{w, UAS-grk.sec/Cyo;}* (BDSC: 58417), *{;UAS-vn^{EPgy}/Cyo;}* (BDSC: 58498), *{;;UAS-krn-3xHA}* (FlyORF: F002754), *{;UAS-bnl/Cyo; MKRS/TM6C}* (BDSC: 64232), *{;UAS-Ilp1;}, {;UAS-Ilp6;}* (gifts from P. Leopold), *{w^{1118}, UAS-Pvf1^{XP};;}* (BDSC: 19632), *{w^{1118}; UAS-Pvf2^{XP};}* (BDSC: 19631), *{;UAS-Wnt4^{EPgy2}/Cyo;}* (BDSC: 20162), *{;;UAS-boss-3xHA}* (FlyORF: F001365), *{y,sev; SAM.dCas9.Trk;}* (BDSC: 81322), *{y,sev; SAM.dCas9.Pvf3;}* (BDSC: 81346), *{y,sev; SAM.dCas9.ths;}* (BDSC: 81347), *{y,sev; SAM.dCas9.pyr;}* (BDSC: 81330), *{w^{1118}; Ddr^{CR01018}-Gal4;}* (BDSC: 81157).

Mosaic analysis:

We generated *ptc^{S2}* MARCM (Fig. 2P) clones by heat-shocking larvae 2 days after egg laying (AEL) at 37°C for 90 minutes. To generate one wild-type MARCM clone per lamina (Fig. S2B,C), we heat-shocked larvae (1 day AEL) for 60 minutes at 37°C. Finally, we induced *Dronc^{I24}* MARCM clones (Fig. S4C) and *Dronc^{I24}, UAS-Yan^{ACT}* MARCM clones (Fig. S4D) by heat-shocking larvae (2 days AEL) for 120 minutes at 37°C. All MARCM crosses were raised at 25°C until dissection at 0-5 hours APF.

Immunocytochemistry, in situ hybridization chain reaction, antibodies and microscopy:

We dissected eye-optic lobe complexes from early pupae (0-5hrs APF) in 1X phosphate-buffered saline (PBS), fixed in 4% formaldehyde for 20 minutes, blocked in 5% normal donkey serum and incubated in primary antibodies diluted in block for 2 nights at 4°C. Samples were then washed in 1X PBS with 0.5% TritonX (PBSTx), incubated in secondary antibodies diluted in block, washed in PBSTx and mounted in SlowFade (Life Technologies).

When performing phospho-MAPK stains, dissections were performed in a phosphatase inhibitor buffer as detailed in[50].

To detect *spi* transcripts by *in situ* hybridization chain reaction, we dissected, fixed and permeabilized the optic lobes as above before following the protocol described in[51].

We used the following primary antibodies in this study: mouse anti-Dac[2-3] (1:20, Developmental Studies Hybridoma Bank; DSHB), mouse anti-Repo (1:20, DSHB), rat anti-Elav (1:100, DSHB), mouse anti-Elav (1:20, DSHB), rabbit anti-Dcp-1 (1:100; Cell Signalling #9578), chicken anti-GFP (1:400; EMD Millipore), mouse anti-Svp (1:50, DSHB), rabbit anti-Slp2 (1:100; a gift from C. Desplan), rabbit-Bsh (1:500; a gift from C. Desplan), Rat anti-Pdm3 (1:1000; a gift from C. Desplan), guinea pig anti-Brp (1:100; a gift from C. Desplan), mouse anti-sim (1:20; a gift from T. Tabata), rabbit anti-Phospho-p44/42 MAPK (Erk1/2) (Thr202/Tyr204) (1:100, Cell Signaling #9101), chicken anti-RFP (1:500; Rockland #600-901-379s), mouse anti β-galactosidase (1:500; Promega # Z3781), chicken anti β-galactosidase (1:500; abcam #9361), rabbit-anti-GFP (1:500; Thermofisher #A6455), AlexaFluor405 conjugated Goat Anti-HRP (1:100; Jackson Immunolabs), AlexaFluor405-, Cy3-, or AlexaFluor647- conjugated Goat Anti-HRP (1:200; Jackson Immunolabs). Secondary antibodies were obtained from Jackson Immunolabs or Invitrogen and used at 1:800. Images were acquired using Zeiss 800 and 880 confocal microscopes with 40X objectives.

Quantification and Statistical analyses:

We used Fiji-ImageJ[52] or Imaris (version x64-9.5.1) to process and quantify confocal images as described below. We used Adobe Photoshop and Adobe Illustrator software to prepare figures. We used GraphPad Prism8 or JMP software to perform statistical tests. In all graphs, whiskers indicate the standard error of the mean (SEM).

Dcp-1 quantifications:

We used the surfaces tool in Imaris to manually select the lamina region (based on Dac expression). We then used the spots tool to identify Dcp-1 positive cells (cell diameter = 5μm) within the selected region using the default thresholding settings, and plotted these values normalised to the volume of the selected lamina region in GraphPad Prism8.

Cell-type quantifications:

LPCs per column: Column number was identified by counting HRP-labelled photoreceptor axon bundles. We considered the youngest column located adjacent to the lamina furrow to be the first column, with column number (age) increasing towards the posterior (right) of the furrow. We counted the number of Dac+ cells per column by quantifying 10 optical slices (step size = 1µm) located centrally in the lamina.

Control vs. *Lamina^{ts}>PntP1:* We quantified the lamina neuron subtypes per column using the following markers to identify L-neuron types: Elav+ and Slp2+ cells were counted as L1-L3s; Elav+ and Bsh+ cells were counted as L4s and Elav+, Bsh+ and Slp2+ cells were counted as L5s. We quantified 10 optical slices (step size = 1µm) located centrally in the lamina. Column number was identified by counting HRP-labelled photoreceptor axon bundles. These quantifications were done blind.

Ligand receptor screen: We quantified the number of L5s based on Elav expression in the proximal lamina. Column number was identified by counting HRP-labelled photoreceptor axon bundles. We quantified 30 optical slices (step size = 1µm) located centrally in the lamina.

Ligand over-expression quantifications: We quantified the number of L-neuron types per column using Elav, Bsh and Slp2. We quantified 30 optical slices (step size = 1µm) located centrally in the lamina. Column number was identified by counting HRP-labelled photoreceptor axon bundles.

Spi Probe Intensity Quantifications:

In Fiji-ImageJ we used the free hand selection tool to draw a region of interest (ROI) around the xg^{O} (marked by the *xg^{O}>CD8::GFP*). We then measured the mean fluorescence intensity of *spi* transcripts labelled by HCR within each ROI. We quantified 30 optical slices (step size = 1µm) located centrally in the lamina and then plotted the average for each optic lobe.

Mean Fluorescence Intensity (MFI) quantifications and statistical analyses:

Using Fiji-ImageJ, we selected the 10 most centrally located optical slices of the lamina (*ptc-lacZ;* Fig. S2D; step size = 1µm) using photoreceptor axons (HRP), and the lobula plug (Dac

expression) as landmarks. We then obtained average intensity projections of these and generated MFI profile plots by measuring β-Gal MFI from the youngest lamina column to the oldest column for each of the 6 rows (distal-proximal cell positions) of the lamina.

We used a mixed effects linear model in JMP to test for an interaction between *ptc-lacZ (β-Gal)* Mean Fluorescence Intensity, distal-to-proximal cell position and Distance posterior to the first column (Summary Statistics are provided in Table S1). We used GraphPad Prism8 to apply a moving average of 6 neighbours to smooth the data, which are plotted in Fig. S2D.

Number of xg^O:

We quantified the number of xg^O (Fig. S3Q) by manually counting the number of Repo positive nuclei within LifeAct-GFP positive xg^O per 40µm optical section in Fiji-ImageJ. We used a step size of 1mm while acquiring the z-stacks and centred each 40µm optical section in the middle of the lamina using photoreceptor axons (HRP), and the lobula plug (Dac expression) as landmarks. Quantifications were performed blind.

Length of xg^O processes:

We quantified the lengths of the fine glial processes that extend distally from the xg^O towards the lamina plexus (Fig. S3O,P,R) by using the straight-line selection and measuring tools in Fiji-ImageJ to measure xg^O process lengths in a 10mm optical section centred in the middle of the lamina. Quantifications were performed blind.

dpMAPK quantifications nuclear to cytoplasmic:

Using Fiji we manually drew regions of interest (ROIs) with the free hand selection tool around the xg^O nucleus (based on Repo) and added these to the ROI manager. We then enlarged the ROIs (Edit>Selection>Enlarge) by 3.00 pixel units to include the cytoplasm. We then used the XOR function in the ROI Manager to only select the cytoplasm of the xg^O. We then measured the MFI of dpMAPK in the nucleus and the cytoplasm of the xg^O in 20 centrally located optical slices (corresponding to 20µm) for each optic lobe. We plotted the nuclear:cytoplasmic ratios of dpMAPK MFI in GraphPad Prism8.

scRNAseq analyses:

To maximize temporal resolution during development as well as the number of cells analysed, we combined three publicly available scRNAseq datasets of optic lobes from the following developmental timepoints: wandering third instar larva, 0 hours after puparium formation (APF), 12 hours APF, 15 hours APF and 24 hours APF. We combined these datasets using the Seurat v.3 integration pipeline to remove batch effects between libraries [53] as follows: Using the default parameters in Seurat 4.0.1 we first normalised each dataset with the NormaliseData function. Next, we extracted the 2000 most variable features with the FindVariableFeatures function. We then integrated the data using the FindIntegrationAnchors and IntegrateData functions. Next, we clustered the integrated dataset using the following functions: ScaleData, RunPCA (using 150 principal components as in [54]), FindNeighbours (80 dimensions), FindClusters (resolution = 5), RunUMAP.

We annotated clusters corresponding to lamina cell types based on a combination of previous annotations from the source datasets [20] and known markers: *dac, eya, tll, gcm* for lamina precursor cells; *svp* and *slp2* for L1s; *slp2* for L2s; *erm* and *slp2 for L3s*; *bsh and apterous for L4s*; *bsh* and *slp2 for L5s* [8,13,18,55–57].

To analyse differentially expressed genes between the L1-L4 and the L5 convergent tails, we first used the CellSelector function to manually select the two tails as two individual clusters. Next, we used the FindMarkers (two-sided Wilcox rank-sum test) function with default parameters to identify positively or negatively expressed genes based on log fold change. To visualise UMAPs and gene expression, we used the DimPlot and FeaturePlot functions.

References

1. Luo, L. & Flanagan, J. G. Development of Continuous and Discrete Neural Maps. *Neuron* **56**, 284–300 (2007).
2. Hidalgo, A. The control of cell number during central nervous system development in flies and mice. **120**, 1311–1325 (2003).
3. Miguel-aliaga, I. & Thor, S. Programmed cell death in the nervous system — a programmed cell fate ? *Curr. Opin. Neurobiol.* **19**, 127–133 (2009).
4. Hadjieconomou, D., Timofeev, K. & Salecker, I. A step-by-step guide to visual circuit assembly in Drosophila. *Curr. Opin. Neurobiol.* **21**, 76–84 (2011).

5. Malin, J. & Desplan, C. Neural specification, targeting, and circuit formation during visual system assembly. *Proc. Natl. Acad. Sci.* **118**, e21018231182 (2021).
6. Treisman, J. E. Retinal differentiation in Drosophila. *Wiley Interdiscip. Rev. Dev. Biol.* **2**, 545–557 (2013).
7. Fischbach, K.-F. & Dittrich, a P. The optic lobe of Drosophila melanogaster. I: A. Golgi analysis of wild-type structure. *Cell Tissue Res* **258**, 441–475 (1989).
8. Huang, Z. & Kunes, S. Hedgehog, transmitted along retinal axons, triggers neurogenesis in the developing visual centers of the Drosophila brain. *Cell* **86**, 411–22 (1996).
9. Huang, Z. *et al.* Signals transmitted along retinal axons in Drosophila: Hedgehog signal reception and the cell circuitry of lamina cartridge assembly. *Development* **125**, 3753–64 (1998).
10. Sugie, A., Umetsu, D., Yasugi, T., Fischbach, K.-F. & Tabata, T. Recognition of pre- and postsynaptic neurons via nephrin/NEPH1 homologs is a basis for the formation of the Drosophila retinotopic map. *Development* **137**, 3303–3313 (2010).
11. Umetsu, D., Murakami, S., Sato, M. & Tabata, T. The highly ordered assembly of retinal axons and their synaptic partners is regulated by Hedgehog/Single-minded in the Drosophila visual system. *Development* **133**, 791–800 (2006).
12. Huang, Z., Shilo, B. Z. & Kunes, S. A retinal axon fascicle uses spitz, an EGF receptor ligand, to construct a synaptic cartridge in the brain of Drosophila. *Cell* **95**, 693–703 (1998).
13. Tan, L. *et al.* Ig Superfamily Ligand and Receptor Pairs Expressed in Synaptic Partners in Drosophila. *Cell* **163**, 1756–1769 (2015).
14. Fernandes, V. M., Chen, Z., Rossi, A. M., Zipfel, J. & Desplan, C. Glia relay differentiation cues to coordinate neuronal development in Drosophila. *Science (80-.).* **357**, 886–891 (2017).
15. Apitz, H. & Salecker, I. A challenge of numbers and diversity: neurogenesis in the Drosophila optic lobe. *J. Neurogenet.* **28**, 1–35 (2014).
16. Akagawa, H., Hara, Y., Togane, Y., Iwabuchi, K. & Hiraoka, T. The role of the effector caspases drICE and dcp-1 for cell death and corpse clearance in the developing optic lobe in Drosophila. *Dev. Biol.* 1–15 (2015). doi:10.1016/j.ydbio.2015.05.013
17. Fuchs, Y. & Steller, H. Programmed Cell Death in Animal Development and Disease. *Cell*

147, 742–758 (2011).

18. Hasegawa, E., Kaido, M., Takayama, R. & Sato, M. Brain-specific-homeobox is required for the specification of neuronal types in the Drosophila optic lobe. *Dev. Biol.* **377**, 90–99 (2013).

19. Konstantinides, N. *et al.* A comprehensive series of temporal transcription factors in the fly visual system. *bioRxiv* 2021.06.13.448242 (2021).

20. Özel, M. N. *et al.* Neuronal diversity and convergence in a visual system developmental atlas. *Nature* **589**, 88–95 (2020).

21. Kurmangaliyev, Y. Z. *et al.* Transcriptional Programs of Circuit Assembly in the Drosophila Visual System. *Neuron* **108**, 1045–1057 (2020).

22. Suzuki, T. *et al.* Formation of Neuronal Circuits by Interactions between Neuronal Populations Derived from Different Origins in the Drosophila Visual Center. *Cell Rep.* **15**, 499–509 (2016).

23. Chen, Y. & Struhl, G. Dual Roles for Patched in Sequestering and Transducing Hedgehog. **87**, 553–563 (1996).

24. Biehs, B., Kechris, K., Liu, S. & Kornberg, T. B. Hedgehog targets in the Drosophila embryo and the mechanisms that generate tissue-specific outputs of Hedgehog signaling. *Development* **137**, 3887–3898 (2010).

25. Albert, E. A., Puretskaia, O. A., Terekhanova, N. V & Labudina, A. Direct control of somatic stem cell proliferation factors by the Drosophila testis stem cell niche. **145**, dev156315 (2018).

26. Busson, D. & Pret, A. GAL4/UAS Targeted Gene Expression for Studying Drosophila Hedgehog Signaling. *Methods Mol. Biol.* **397**, 161–201 (2007).

27. Kalderon, D. The mechanism of hedgehog signal transduction. *Biochem. Soc. Trans.* **33**, 1509–1512 (2005).

28. Lee, T. & Luo, L. Mosaic analysis with a repressible cell marker (MARCM) for Drosophila neural development. *Trends Neurosci.* **24**, 251–4 (2001).

29. Edwards, T. N., Nuschke, A. C., Nern, A. & Meinertzhagen, I. a. Organization and metamorphosis of glia in the Drosophila visual system. *J. Comp. Neurol.* **520**, 2067–2085 (2012).

30. Chotard, C. & Salecker, I. Glial cell development and function in the Drosophila visual

system. *Neuron Glia Biol.* **3**, 17–25 (2007).

31. Yogev, S., Schejter, E. D. & Shilo, B. Z. Polarized secretion of drosophila EGFR ligand from photoreceptor neurons is controlled by ER localization of the ligand-processing machinery. *PLoS Biol.* **8**, e1000505 (2010).
32. Sopko, R. & Perrimon, N. Receptor tyrosine kinases in Drosophila development. *Cold Spring Harb Perspect Biol.* **5**, a009050 (2013).
33. Freeman, M., Klämbt, C., Goodman, C. S. & Rubin, G. M. The argos gene encodes a diffusible factor that regulates cell fate decisions in the drosophila eye. *Cell* **69**, 963–975 (1992).
34. Golembo, M., Schweitzer, R., Freeman, M. & Shilo, B. argos transcription is induced by the Drosophila EGF receptor pathway to form an inhibitory feedback loop. *Development* **230**, 223–230 (1996).
35. Jenett, A. *et al.* A GAL4-driver line resource for Drosophila neurobiology. *Cell Rep.* **2**, 991–1001 (2012).
36. Placzek, M. & Briscoe, J. Sonic hedgehog in vertebrate neural tube development. *Int. J. Dev. Biol.* **62**, 225–234 (2018).
37. Sagner, A. & Briscoe, J. Establishing neuronal diversity in the spinal cord : a time and a place. *Development* **146**, dev182154 (2019).
38. Viktorin, G., Riebli, N. & Reichert, H. A multipotent transit-amplifying neuroblast lineage in the central brain gives rise to optic lobe glial cells in Drosophila. *Dev. Biol.* **379**, 182–194 (2013).
39. Ren, Q., Awasaki, T., Wang, Y., Huang, Y. & Lee, T. Lineage-guided Notch-dependent gliogenesis by Drosophila multi-potent progenitors. *Development* **145**, dev160127 (2018).
40. Franzdóttir, S. R. *et al.* Switch in FGF signalling initiates glial differentiation in the Drosophila eye. *Nature* **460**, 758–761 (2009).
41. Pinto-teixeira, F., Konstantinides, N. & Desplan, C. Programmed cell death acts at different stages of Drosophila neurodevelopment to shape the central nervous system. *FEBS Lett.* **590**, 2435–2453 (2016).
42. Yamaguchi, Y. & Miura, M. Review Programmed Cell Death in Neurodevelopment. *Dev. Cell* **32**, 478–490 (2015).
43. Davies, A. M. Regulation of neuronal survival and death by extracellular signals during

development. *EMBO J.* **22**, 2537–2545 (2003).

44. Ballif, B. A. & Blenis, J. Molecular Mechanisms Mediating Mammalian Mitogen-activated Protein Kinase (MAPK) Kinase (MEK)-MAPK Cell Survival Signals. *Cell Growth Differ.* **12**, 397–408 (2001).
45. Park, H. & Poo, M. M. Neurotrophin regulation of neural circuit development and function. *Nat. Rev. Neurosci.* **14**, 7–23 (2013).
46. Kurada, P. & White, K. Ras Promotes Cell Survival in Drosophila by Downregulating hid Expression. **95**, 319–329 (1998).
47. Bergmann, A., Agapite, J., McCall, K. & Steller, H. The Drosophila gene hid is a direct molecular target of Ras-dependent survival signaling. *Cell* **95**, 331–41 (1998).
48. Bergmann, A., Tugentman, M., Shilo, B. Z. & Steller, H. Regulation of cell number by MAPK-dependent control of apoptosis: A mechanism for trophic survival signaling. *Dev. Cell* **2**, 159–170 (2002).
49. Zang, Y. *et al.* Plasma membrane overgrowth causes fibrotic collagen accumulation and immune activation in Drosophila adipocytes. *Elife* **4**, e07187 (2015).
50. Amoyel, M., Anderson, J., Suisse, A., Glasner, J. & Bach, E. A. Socs36E Controls Niche Competition by Repressing MAPK Signaling in the Drosophila Testis. *PLoS Genet.* **12**, e1005815 (2016).
51. Duckhorn, J. C., Junker, I., Ding, Y. & Shirangi, T. R. Combined in situ hybridization chain reaction and immunostaining to visualize gene expression in whole-mount Drosophila central nervous. *bioRxiv* 2021.08.02.454831 (2021).
52. Schindelin, J. *et al.* Fiji : an open-source platform for biological-image analysis. *Nat Methods* **9**, 676–682 (2012).
53. Stuart, T. *et al.* Comprehensive Integration of Single-Cell Data Resource Comprehensive Integration of Single-Cell Data. *Cell* **177**, 1888-1902.e21 (2019).
54. Konstantinides, N. *et al.* A comprehensive series of temporal transcription factors in the fly visual system. *bioRxiv* **06**, 448242 (2021).
55. Chotard, C., Leung, W. & Salecker, I. glial cells missing and gcm2 cell autonomously regulate both glial and neuronal development in the visual system of Drosophila. *Neuron* **48**, 237–251 (2005).
56. Guillermin, O., Perruchoud, B., Sprecher, S. G. & Egger, B. Characterization of Tailless

functions during drosophila optic lobe formation. *Dev. Biol.* **405**, 202–213 (2015).

57. Piñeiro, C., Lopes, C. S. & Casares, F. A conserved transcriptional network regulates lamina development in the Drosophila visual system. *Development* **141**, 2838–47 (2014).

Acknowledgements:

We thank C. Desplan, A. Gould, D. Kalderon, B. Shilo, G. Stuhl and J. Treisman for reagents, and S. Ackerman, M. Amoyel, B. Conradt, C. Desplan, C. Doe, A. Franz, P. Salinas, A. Rossi, C. Stern, L. Venkatasubramanian and members of the Amoyel and Fernandes labs for comments on the manuscript. Stocks obtained from the Bloomington Drosophila Stock Center (NIH P40OD018537) were used in this study. Monoclonal antibodies obtained from the Developmental Studies Hybridoma Bank, created by the NICHD of the NIH and maintained at The University of Iowa, were used in this study.

Funding:

Wellcome Trust Sir Henry Dale Research Fellowship 210472/Z/18/Z (VMF), UCL Overseas Research Scholarship (ARP) and UCL Graduate Research Scholarship (ARP).

Author contributions:

Conceptualization: VMF, ARP, MPB

Investigation: ARP, MPB, ILB, ZH, VMF

Supervision: VMF

Writing – original draft: VMF

Writing – review & editing: ARP, MPB, ILB

Competing interests:

The authors declare no competing interests.

1 **Fig. 1**

2

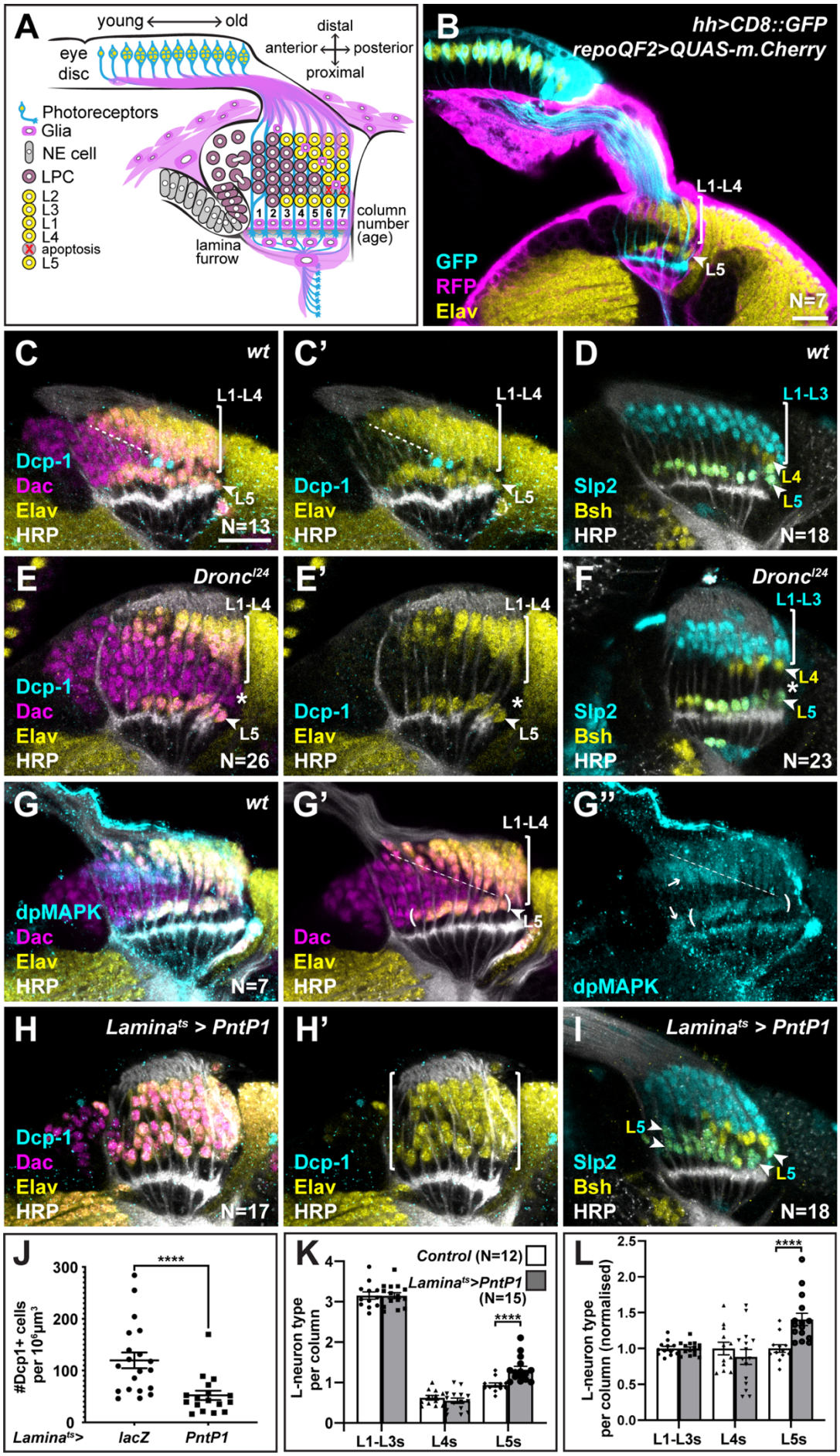

Fig. 1: The 'extra' LPCs are specified as L5s

(A) Schematic of the developing lamina. Photoreceptors (blue) drive lamina precursor cell (LPC; purple) birth from neuroepithelial cells (NE; grey) and their assembly into columns of ~6 LPCs, which differentiate into the L1-L5 neurons (yellow) following an invariant spatiotemporal pattern. The 'extra' LPC is cleared by apoptosis (red X). Several glial types (magenta) associate with the lamina. **(B)** A cross-sectional view of an early pupal (0-5 hours APF) optic lobe where *hh-Gal4* drives *UAS-CD8::GFP* expression in photoreceptors (cyan). The pan-glial driver *repo-QF2* drives *QUAS-m.Cherry* (magenta) in all glia. Elav (yellow) marks all neurons. **(C,D)** Wild-type optic lobes stained for **(C)** Dac (lamina cell bodies; magenta), Horseradish peroxidase (photoreceptor axons; HRP; white), Elav (neurons; yellow) and cleaved Dcp-1 (apoptotic cells; cyan). Dcp-1 positive cells are located between L1-L4s and L5s and correspond to the 'extra' LPCs, which are being eliminated. **(D)** HRP (white) and L-neuron subtype specific markers Slp2 (cyan) and Bsh (yellow), which individually mark L1-L3 and L4s respectively, and are co-expressed in L5s. **(E,F)** *Dronc*^{I24} optic lobes stained for the same markers as in (C) and (D), respectively. **(E)** No Dcp-1 positive cells were recovered and Dac positive cells between L1-L4s and L5s persisted into the oldest columns. **(F)** A space (negative for both markers; asterisk) was present between L4s and L5s. **(G)** Wild-type optic lobes stained for Dac (magenta), HRP (white), Elav (yellow) and dpMAPK (cyan). dpMAPK levels were high (arrows in G") just prior to Elav expression (dashed line for the front of L1-L4 differentiation and brackets for L5 differentiation). **(H,I)** Optic lobes with lamina-specific overexpression of PntP1 stained as in (C) and (D), respectively. **(H)** Fewer Dcp-1 positive cells were recovered compared with controls. **(I)** Roughly two rows of Slp2 and Bsh co-expressing cells (L5s) were recovered (arrow heads). **(J)** Quantification of the number of Dcp-1 positive cells in (H) compared with control *Lamina*^{ts}*>lacZ* (Figure S1A) (P<0.0001; Mann-Whitney U test; error bars indicate standard error of the mean; SEM). **(K)** Quantification of the number of L-neuron types per column based on Slp2 and Bsh expression from column 7 onwards shows an increase in the number of L5s/column in *Lamina*^{ts}*>PntP1* compared with controls; P<0.0001; Mann-Whitney U test. **(L)** Same as (K) but normalised to the mean of the control. The number of L5s/column in *Lamina*^{ts}*>PntP1* increase ~1.4 fold relative to controls; P <0.0001; Mann-Whitney U test. Error bars indicate SEM. Ns indicated in parentheses for J,K. Scale bar = 20µm.

Fig. 2

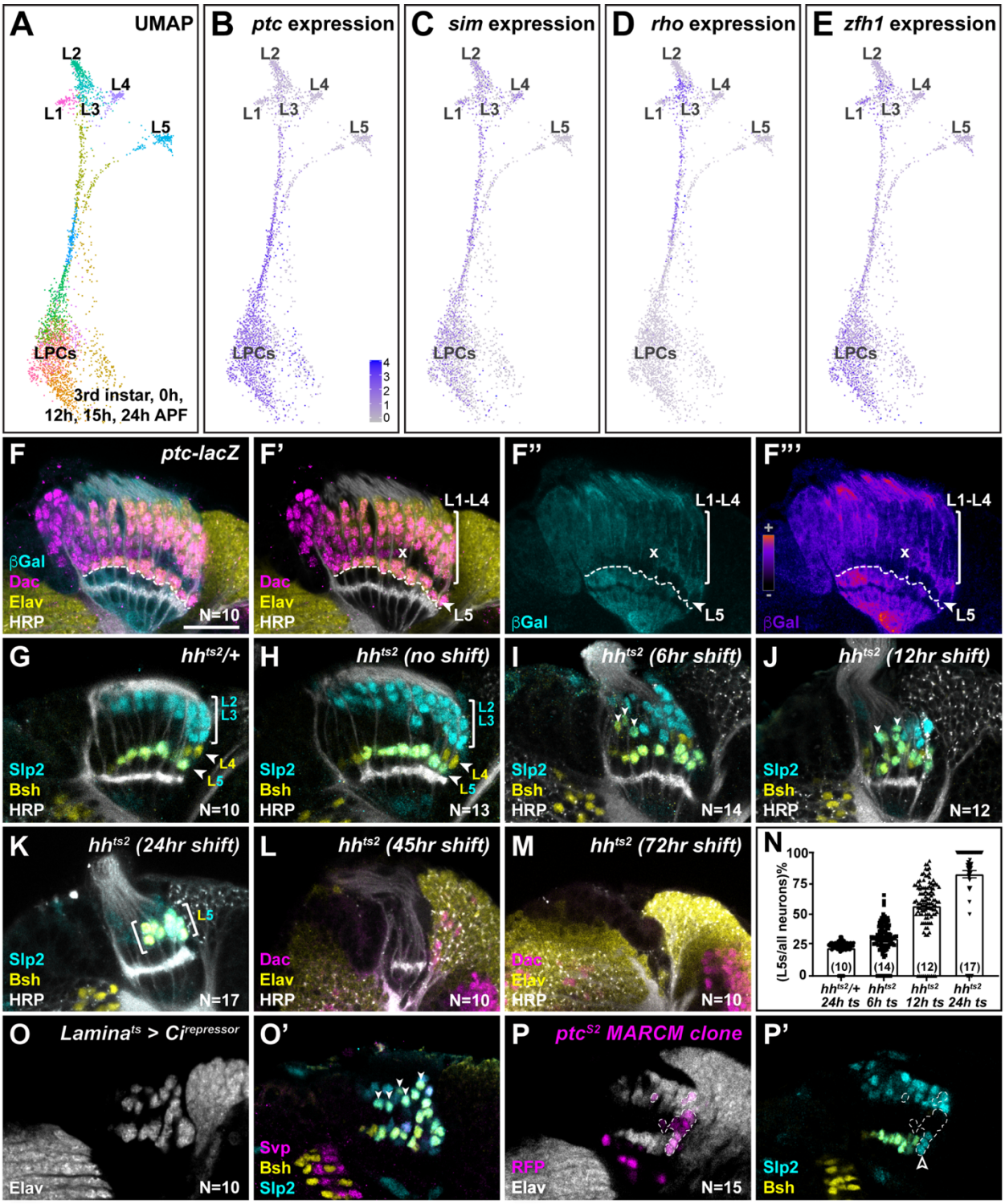

Fig. 2: Hh signalling patterns LPCs

(A) UMAP visualisation of LPCs, differentiated L1-L5 neurons and intermediate stages of differentiation using 150 principal components calculated on the log-normalized integrated gene expression from single-cell RNA sequencing datasets of the third larval instar, 0 hours-, 12 hours-, 15 hours- and 24 hours-APF [19–21]. See Figure S2A for full integrated dataset. **(B-E)** UMAP visualisation from (A; grey) showing log normalised expression of the Hh signalling targets (blue): **(B)** *ptc*, **(C)**, *sim*, **(D)** *rho* and **(E)** *zfh1,* which all show higher levels of expression in the convergent tail connecting the LPC cluster with mature L1-L4 neuron clusters rather than the tail connecting the LPC cluster with the L5 neuron cluster. **(F)** An optic lobe expressing *ptc-LacZ* stained for β-Galactosidase (β-Gal; cyan), Dac (magenta), Elav (yellow) and HRP (white). **(F"')** shows (F") in pseudo-colour. Dashed line marks the most proximal surface of the lamina. "x" marks the point from which the 'extra' LPCs have been cleared. In young columns, β-Gal expression decreases along the distal to proximal axis, being lowest in the proximal lamina. L5s have the lowest levels of β-Gal, which eventually decreases in older L1-L4s; quantified in Figure S2D with summary statistics in Table S2. **(G-K)** HRP (white) and lamina neuron subtype specific markers Slp2 (cyan) and Bsh (yellow) from: **(G)** hh^{ts2}/+ shifted from the permissive temperature (18ºC) to the restrictive temperature (29ºC) for 24 hours, **(H)** hh^{ts2} raised at the permissive temperature, **(I-K)** hh^{ts2} shifted from the permissive temperature to the restrictive temperature for **(I)** 6 hours, **(J)** 12 hours, **(K)** hh^{ts2} 24 hours. **(I-K)** The pattern of neuronal differentiation worsened progressively with longer temperature shifts, with fewer neurons differentiating overall (quantified in Figure S2F). Slp2 and Bsh positive cells (L5s) were observed in the distal lamina (arrowheads), till most cells present differentiated into L5 neurons for the 24 hour temperature shift. **(L,M)** hh^{ts2} shifted from the permissive temperature to the restrictive temperature for **(L)** 45 hours and **(M)** 72 hours stained for Dac (magenta), Elav (yellow) and HRP (white). A few photoreceptor bundles are present but no LPCs formed under the **(L)** 45 hour temperature shift condition, whereas neither photoreceptors nor LPCs were present for the **(M)** 72 hour temperature shift condition. **(N)** Quantification of the percentage of neurons that differentiated as L5s for (G, I-K). Ns indicated in parentheses. Error bars indicate SEM. **(O)** Lamina-specific misexpression of $Ci^{repressor}$ stained for **(O)** Elav (white) and **(O')** L-neuron subtype specific markers Slp2 (cyan), Bsh (yellow) and Svp (which is expressed in L1s; magenta). Fewer L-neurons were observed and the pattern of neuronal differentiation was

perturbed. As well, Slp2 and Bsh co-expressing cells (L5s) were recovered in the distal lamina (arrowheads). **(P)** An optic lobe with RFP positive *ptc*^{S2} MARCM clones stained for **(P)** Elav (white) and RFP (magenta) **(P')** Slp2 (cyan) and Bsh (yellow). Clones in the lamina are outlined by dashed lines. A clone that spanned the proximal lamina was still Elav and Slp2 positive but lacked Bsh, indicating that the cells had differentiated into L1s, L2s or L3s but not L4s or L5s. Scale bar = 20μm.

Fig. 3

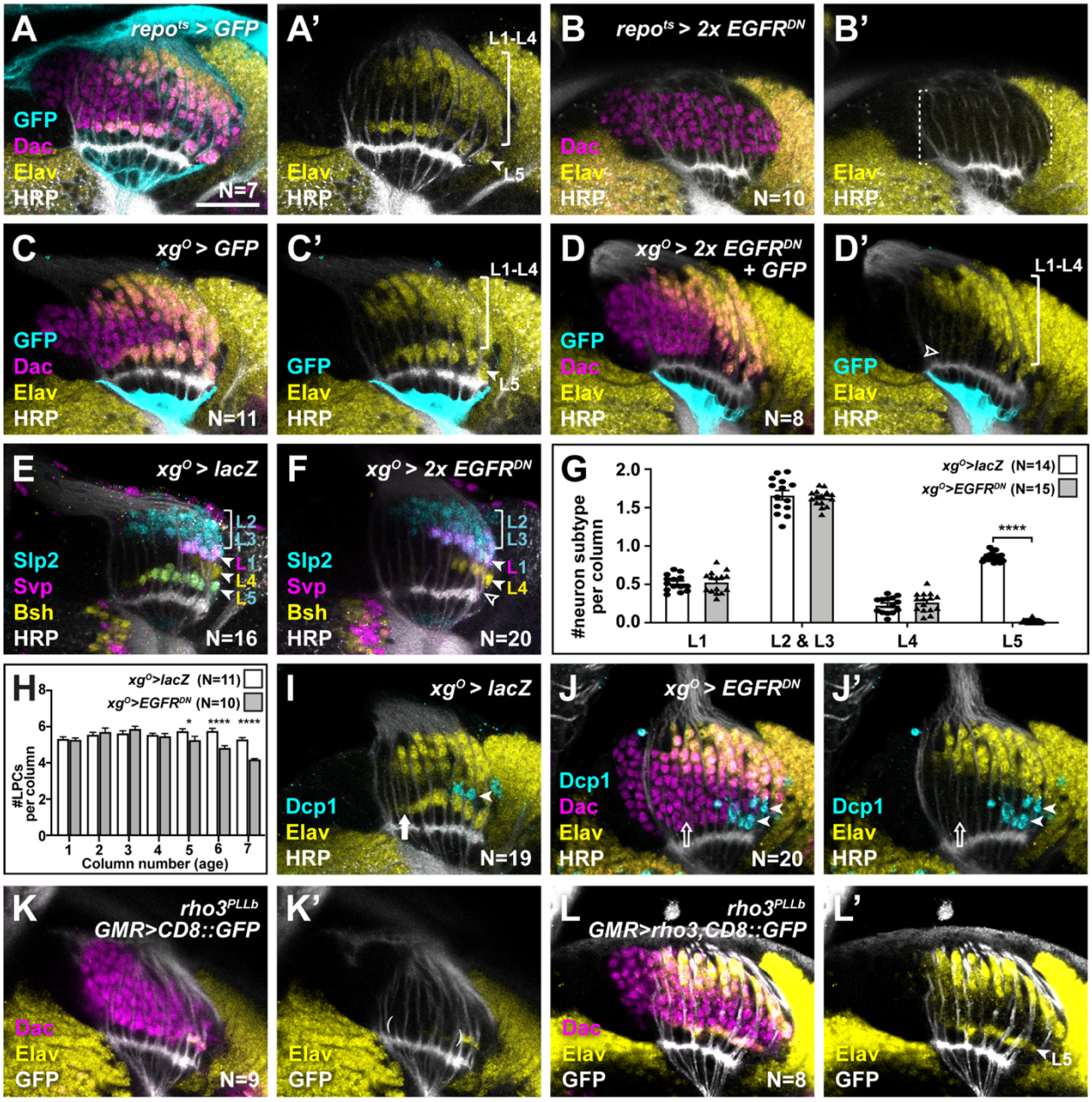

Fig. 3: Outer chiasm giant glia induce L5 neuronal differentiation in response to EGF from photoreceptors

(A) A cross-sectional view of an optic lobe with pan-glial expression of CD8::GFP stained for GFP (cyan), Dac (magenta), Elav (yellow) and HRP (white). **(B)** Pan-glial expression of 2 copies of $EGFR^{DN}$ stained for Dac (magenta), Elav (yellow) and HRP (white). Although LPCs (Dac+ cells) formed, they did not differentiate (lack of Elav+ cells). **(C)** xg^{O}-specific expression of CD8::GFP stained for GFP (cyan), Dac (magenta), Elav (yellow) and HRP (white). **(D)** xg^{O}-specific expression of 2 copies of $EGFR^{DN}$ and CD8::GFP stained for GFP (cyan), Dac (magenta), Elav (yellow) and HRP (white). The number of Elav+ cells in proximal row (L5s) was decreased (empty arrowhead). **(E,F)** HRP (white) and L-neuron subtype specific markers Slp2 (cyan), Bsh (yellow) and Svp (magenta) in **(E)** Control $xg^{O}>lacZ$ optic lobe and **(F)** $xg^{O}>2xEGFR^{DN}$. The number of cells co-expressing Slp2 and Bsh (L5s) was reduced. **(G)** Quantification of the number of L-neuron subtypes per column for control and $xg^{O}>2xEGFR^{DN}$. Only L5 neurons were decreased significantly ($P^{L5}<0.0001$; Mann-Whitney U test. Error bars indicate SEM. Ns indicated in parentheses). **(H)** Quantification of the number of LPCs/column (*i.e.* Dac+ cells/column) for control and $xg^{O}>2xEGFR^{DN}$ showed that a significant decrease was observed only from column 5 onwards (P*<0.05, P****<0.0002; Mann-Whitney U test. Error bars indicate SEM. Ns indicated in parentheses). **(I)** Control $xg^{O}>lacZ$ optic lobe stained for Dcp-1 (cyan), Elav (yellow) and HRP (white). Dcp-1+ cells were always observed just distal to the most proximal row of cells (L5s). **(J)** $xg^{O}>EGFR^{DN}$ stained for Dcp-1 (cyan), Dac (magenta) Elav (yellow) and HRP (white). Dcp-1 positive cells were observed in the most proximal row of LPCs as well as the row just distal to these, starting from column 5.93 ±0.18SEM. **(K)** GMR-Gal4 driven CD8::GFP expression in photoreceptors in a $rho3^{PLLb}$ background stained for GFP (white), Dac (magenta), Elav (yellow). Few proximal Elav+ cells (L5s) were recovered in older columns only as previously published [14]. **(L)** GMR-Gal4 driven Rho3 and CD8::GFP in a $rho3^{PLLb}$ background stained for GFP (white), Dac (magenta), Elav (yellow) showed that L5 neuronal differentiation was rescued (Elav+ cells in the proximal lamina). Scale bar = 20µm.

Fig. 4

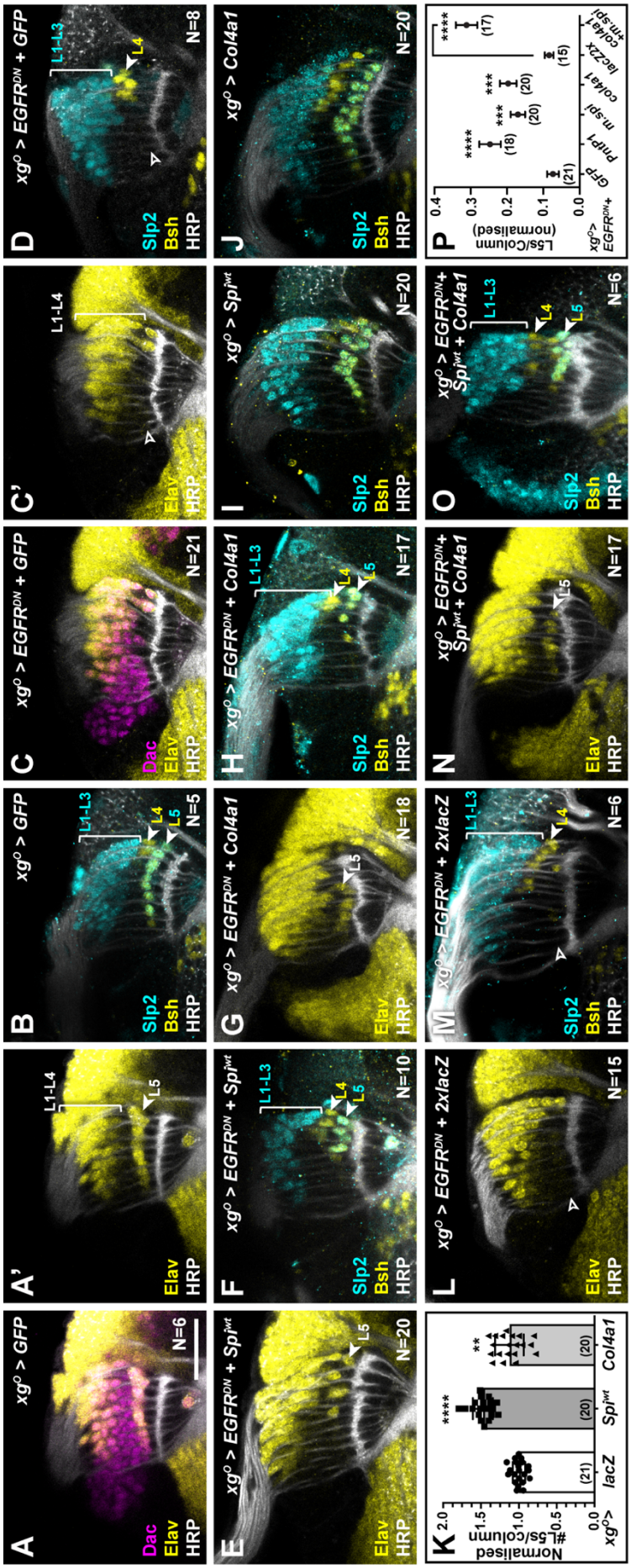

Fig. 4: Xg^{O} secrete multiple ligands to induce L5 neuronal differentiation

(A,B) Control *xg^{O}>GFP* optic lobes. **(A)** Dac (magenta), Elav (yellow) and HRP (white) or **(B)** HRP (white) and L-neuron specific markers Slp2 (cyan) and Bsh (yellow). **(C,D)** Gal4 titration control *xg^{O}>GFP+$EGFR^{DN}$* **(C)** Dac (magenta), Elav (yellow) and HRP (white). Elav+ cells were reduced in number in the proximal lamina. **(D)** HRP (white) and L-neuron specific markers Slp2 (cyan) and Bsh (yellow). The number of Slp2 and Bsh co-expressing cells was reduced. **(E,F)** Wild-type Spi (Spi^{wt}) co-expression with $EGFR^{DN}$ specifically in xg^{O}. **(E)** stained for Elav (yellow) and HRP (white). Some Elav+ cells were recovered in the proximal lamina **(F)** HRP (white) and L-neuron specific markers Slp2 (cyan) and Bsh (yellow). Slp2 and Bsh co-expressing cells were recovered in the proximal lamina. **(G,H)** Col4a1 co-expression with $EGFR^{DN}$ specifically in xg^{O}. **(G)** stained for Elav (yellow) and HRP (white). Some Elav+ cells were recovered in the proximal lamina **(H)** HRP (white) and L-neuron specific markers Slp2 (cyan) and Bsh (yellow). Slp2 and Bsh co-expressing cells were recovered in the proximal lamina. **(I,J)** Optic lobes stained for Slp2 and Bsh when xg^{O} overexpress **(I)** Spi^{wt} or **(J)** Col4a1. In both instances, ectopic Slp2 and Bsh co-expressing cells (L5s) are recovered in the proximal lamina. **(K)** Quantification of the number of L5s/column from (I-J) normalised to the control *xg^{O}>lacZ*. ($P^{spi.wt}$<0.0001; P^{Col4a1}<0.01; Mann-Whitney U test. Error bars indicate SEM. Ns indicated in parentheses). **(L,M)** Gal4 titration control *xg^{O}>$EGFR^{DN}$+2xlacZ* stained for **(L)** Elav (yellow) and HRP (white) or **(M)** HRP (white), Slp2 (cyan) and Bsh (yellow). **(N,O)** Wild-type Spi^{wt} and Col4a1 co-expression with $EGFR^{DN}$ specifically in xg^{O}. **(N)** stained for Elav (yellow) and HRP (white). Elav+ cells were recovered in the proximal lamina **(O)** HRP (white) and L-neuron specific markers Slp2 (cyan) and Bsh (yellow). Slp2 and Bsh co-expressing cells were recovered in the proximal lamina. **(P)** Quantification of the number of L5s/column for the genotypes indicated normalised to the appropriate titration control *xg^{O}>lacZ.* (P^{***}<0.0005; P^{****}<0.0001; Mann-Whitney U test. Error bars indicate SEM. Ns indicated in parentheses). Scale bar = 20µm.

Fig. 5

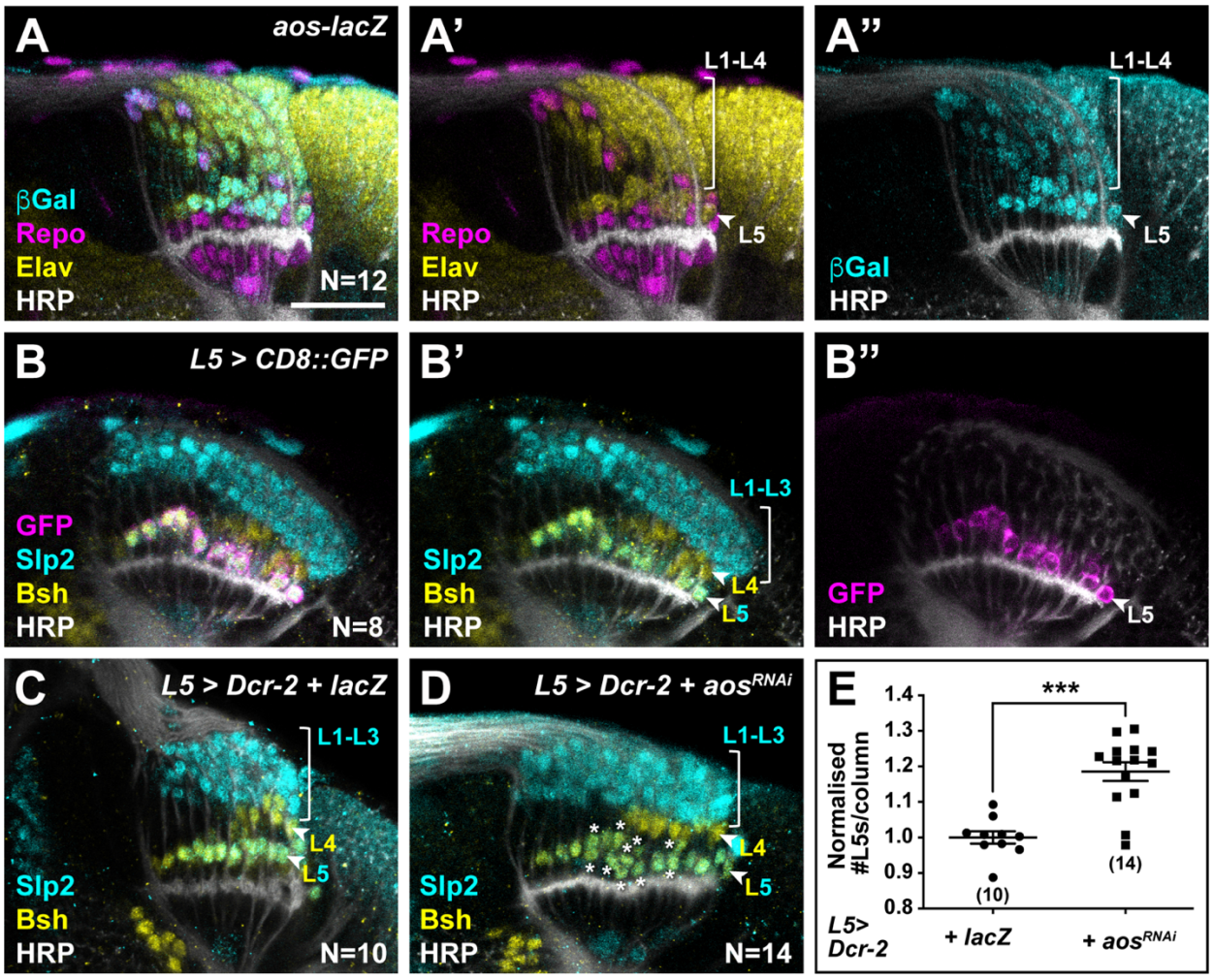

Fig. 5: Newly-induced L5 neurons secrete Aos to limit inductive signals from xg^{O}

(A) *aos-lacZ* expression in the lamina with β-Gal (cyan), Repo (magenta), Elav (yellow), HRP (white). The highest levels of β-Gal expression were observed in proximal LPCs (L5s). Ectopic Elav+ cells were observed in the proximal lamina. **(B)** An L5-specific Gal4 was used to drive GFP (magenta) expression in the lamina; HRP (white) and L-neuron subtypes Slp2 (cyan) and Bsh (yellow). GFP was observed specifically in Slp2 and Bsh co-expressing cells (L5s) with low levels in the youngest neurons. **(C,D)** Optic lobes stained for HRP (white), Slp2 (cyan) and Bsh (yellow) in **(C)** Control *L5>Dcr-2+lacZ* and **(D)** when Dcr-2 and aos^{RNAi} were expressed in developing L5 neurons specifically, which led to an increase in the number of Slp2 and Bsh co-expressing cells (L5s). **(E)** Quantification of the number of L5s/column normalised for (D) and (E) normalised to control (D). (P***<0.0005; Mann-Whitney U test. Error bars indicate SEM. Ns indicated in parentheses). Scale bar = 20μm.

1 **Fig. 6**

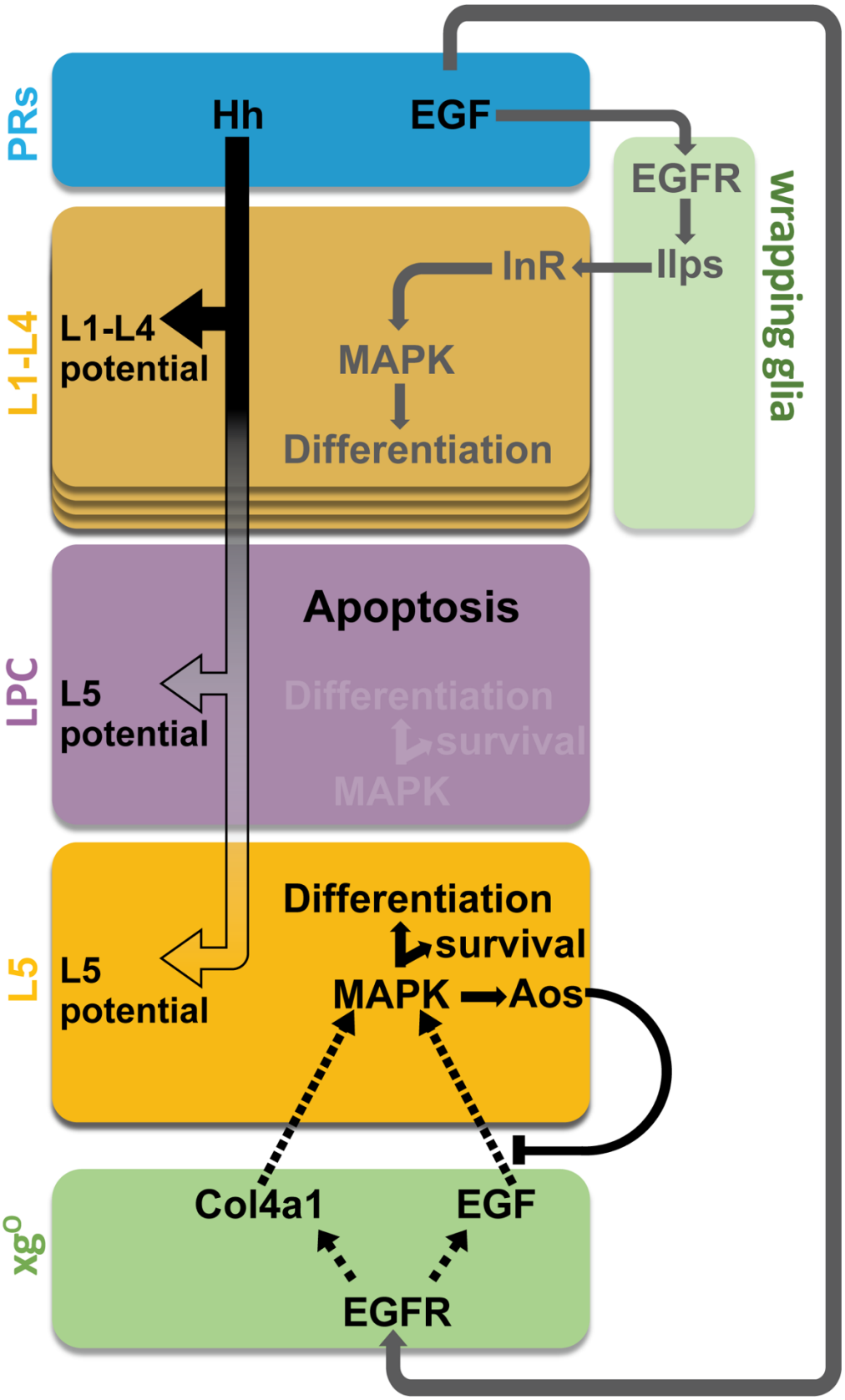

Fig. 6: Summary schematic of neuronal differentiation in the lamina

In our model of lamina neuronal differentiation, differential Hh signalling along the distal-proximal length of lamina columns specifies neuronal identity such that cells with high Hh signalling activity take on distal neuronal identities while those with low Hh signalling levels take on proximal neuronal identity. EGF from photoreceptors activates EGFR signalling in wrapping glia, which induce L1-L4 differentiation, and in xg^{O}, which induce L5 differentiation. Only a subset of the LPCs specified as L5s differentiate (*i.e.* those in the proximal row). We propose that this selective neuronal induction of L5s is due to tissue architecture and feedback from the newly born L5s, which limit available EGF (Spi) by secreting the antagonist Aos.